Vietnam Journal of Earth Sciences, 46(2), 147-167, https://doi.org/10.15625/2615-9783/20010

Vietnam Journal of Earth Sciences
https://vjs.ac.vn/index.php/jse

Delineating geological structure utilizing integration of remote sensing and gravity data: a study from Halmahera, North Molucca, Indonesia

Patria Ufaira Aprina[1*], Djoko Santoso[1,2], Susanti Alawiyah[1,2], Nugroho Prasetyo[1,3], Khalil Ibrahim[1]

[1]*Geophysical Engineering, Faculty of Mining and Petroleum Engineering, Institut Teknologi Bandung, West Java 40132, Indonesia*
[2]*Applied Geophysics and Exploration Research Group, Faculty of Mining and Petroleum Engineering, Institut Teknologi Bandung, West Java 40132, Indonesia*
[3]*Geophysical Engineering, Faculty of Industrial Technology, Institut Teknologi Sumatera, South Lampung 35365, Indonesia*

Received 10 August 2023; Received in revised form 27 November 2023; Accepted 25 January 2024

ABSTRACT

Halmahera Island is the result of the interaction between the Indo-Australian Plate, the Molucca Sea Plate, and the Philippine Plate, which gave rise to many active geological structures that are vulnerable to seismic activity around the island. The complexity of this geological structure makes Halmahera Island very interesting to study. This study aims to identify geological structures by integrating remote sensing and gravity satellite data. Surface lineament analysis using the remote sensing method was carried out based on Sentinel-1A imagery data. The gravity method uses GGMPlus satellite data to clarify the continuity of geological structures that cannot be clearly mapped on the surface. Lineament analysis on gravity data uses techniques such as fast sigmoid edge detection (FSED) and Euler deconvolution. The results of lineament interpretation based on integrating remote sensing and gravity satellite data show that the NE-SW structure controls the northern and northeastern arms of Halmahera.

In contrast, the southern arm is dominated by the NW-SE structure. The Euler depth estimation shows that the Halmahera area contributes to having geological structures at various depths. Deep structures reach 4 km, while shallow structures are found at depths of up to 2 km. Earthquake hypocenter data strengthen the interpretation of this geological structure. This comprehensive study yields an excellent correlation between gravity and remote sensing techniques in describing the general structural framework of the area. The new finding is an NE-SW trending geological structure on the northern Halmahera arm, which may be caused by two different tectonics first, the subduction of the Molucca Sea Plate with the Halmahera Plate in the west. Second, the strike-slip movement is trending NE-SW, which cuts the northern and northeastern arms due to the rotational movement of the thrust fault with the Philippine Plate to the west.

Keywords: Halmahera, remote sensing, gravity, structure, Indonesia.

1. Introduction

Halmahera Island is one of the parts of the Indonesian Archipelago that has geological complexity and lies over the three major conjunction plates: The Eurasian Plate, The Australian Plate, and The Pacific Plate in the west, south, and east, respectively (Fig. 1) (Rangin et al., 1999; Bird, 2003; van Gorsel,

*Corresponding author, Email: patriaufaira@gmail.com

2018). These plate propagations probably cause the geological structures to rise, which is considered a source of seismic activity. Tectonic movements, an eastward Molucca Sea Plate collision, are located approximately 100 km below the Halmahera and generated a strong earthquake on February 26, 2020, with a magnitude of 5.2, equal to the V MMI scale (Rachman et al., 2022). An earthquake occurred on April 18, 2022, with a magnitude of 5.2, produced by an active fault. It caused several damages, collapsed a building, and injured people in Tobelo, North Halmahera (BNPB, 2022). Eastward subduction beneath the Halmahera arc occurs at an angle of 450 and depths reaching approximately 230 km, as Cardwell and Karig (1980) reported. However, recent investigations indicate that the slab is at a depth of around 400 km (Puspito and Hirahara, 1993; Hall and Spakman, 2015; Zenonos et al., 2019).

Seismic activities recorded in the region indicate the presence of numerous active geological structures beneath Halmahera. Several researchers have effectively delineated geological features, such as lineaments and surface fault structures, using remote sensing approaches with Synthetic Aperture Radar (SAR) data (Elhag et al., 2019; Mohcine et al., 2022). The broad coverage of these SAR images facilitates comprehensive observations of regional-scale geological structures. Successful fault interpretations using Sentinel-1A imagery extraction have been applied in various fields (Ahmadi and Pekkan, 2021; Ghosh et al., 2021; Dhara et al., 2022), including the work of Khakim et al. (2023) to investigate ground surface subsidence in Jakarta; Menichetti et al. (2023) for identifying rupture at Mts. Sibilini and Mt. Etna Volcano and Vajedian et al. (2023) map the fault distribution causing displacement in Kerman using Sentinel-1A. However, it should be noted that remote sensing imagery only provides a representation of surface conditions, which may not accurately represent the geological settings. Subsurface faults and those obscured by vegetation or other materials are challenging to interpret using satellite imagery. Due to these facts, this research combined remote sensing and gravity data to elucidate subsurface structures not identified by remote sensing data.

Source edges help map the boundaries of anomalous sources. Edge detection techniques can map the structure's lineament (Pham et al., 2023). Eldosouky et al. (2020, 2022), Prasad et al. (2020), Oksum et al. (2021), Nzeuga et al. (2022), Pham et al. (2021, 2022, 2023), and Alvandi et al. (2023) have put this approach into action and tested how well it works, especially when it comes to finding the edges of gravity and magnetic anomaly bodies. This research aims to use one of the edge detection techniques introduced by Oksum et al. (2021), namely fast sigmoid edge detection (FSED), to be applied to real gravity data in mapping main structural lineaments. The FSED is a method for detecting subsurface rock masses at varying depths, supported by subsequent studies (Altinoğlu, 2023; Kamto et al., 2023; Pham et al., 2023). Furthermore, the Euler approach is utilized to approximate the location of an anomalous source (Thompson, 1982; Reid et al., 1990; Marson and Klingele, 1993; Cooper, 2004; Chen et al., 2022; Pham et al., 2023). This method is expected to accommodate geological structures at continuous depths that the FSED technique cannot accommodate.

The geological structural interpretation in our study is supported by the validation process, which utilizes earthquake hypocentre data. It is postulated that geological structures can be identified as areas of reduced strength that have the potential to undergo displacement. Consequently, the release of energy from these structures can initiate seismic events (Haiyun and Xiaxin, 2003; Dong and Luo, 2022). Halmahera's extensive and isolated geographical area poses

difficulties when carrying out direct evaluations. This study utilizes satellite data from gravity and imagery databases to identify, analyze, and evaluate the geological structure of Halmahera, located in the North Molucca region. The application of satellite data offers valuable insights into Halmahera's geological and geophysical attributes, obviating the necessity for expensive and intricate physical investigation methods. This study employs a regional methodology and aims to investigate the trends of lineaments and geological formations in the Halmahera region of North Molucca. Moreover, the findings of this study are considered to serve as a valuable resource for informing decision-making processes in diverse domains, such as catastrophe mitigation, geological mapping, and environmental mapping.

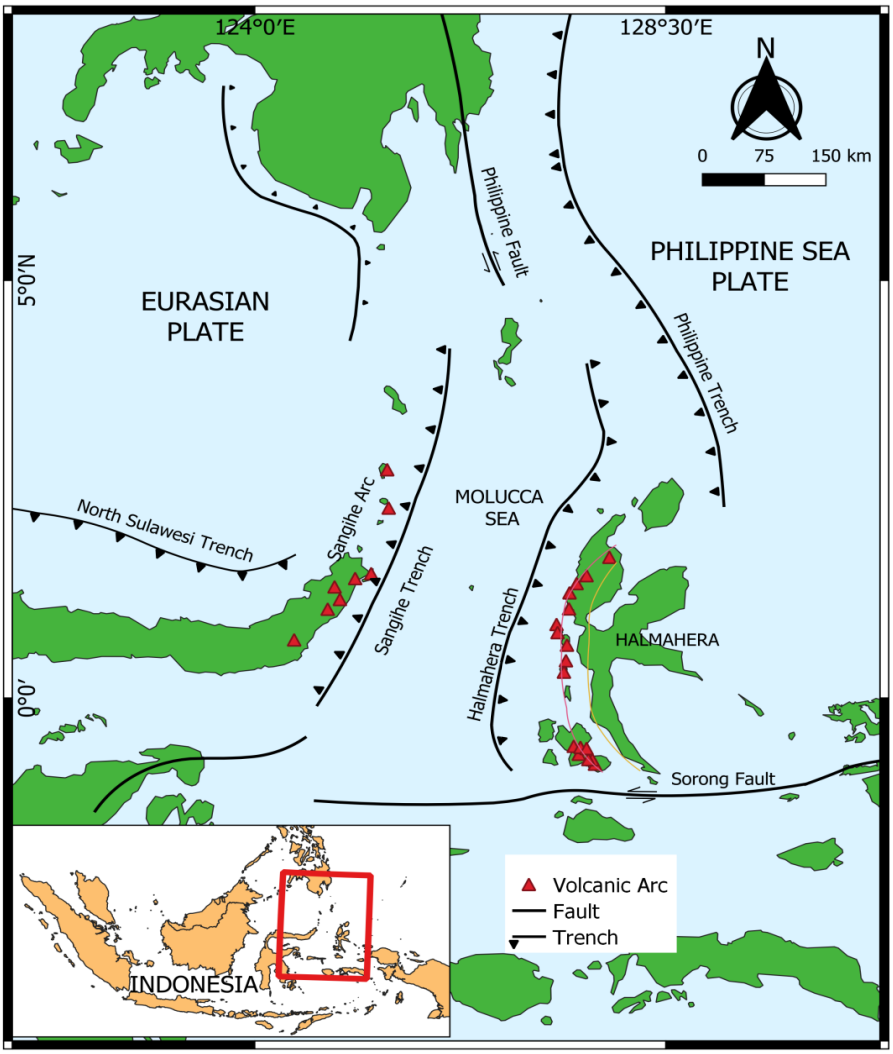

Figure 1. The location of Halmahera is located in three active subduction zones: the western part is bounded by a volcanic arc, which is a product of the Eurasian collision with the Halmahera Plate; the eastern part contains the Philippine Trench; and the strike-slip fault in the southern part is an accommodation for the collision of the Pacific microcontinent with Indo-Australia (modified from van Gorsel, 2018)

2. Geological Settings

From a geotectonic perspective, the island of Halmahera is characterized by the presence of a subduction belt in its western region, subduction of the Philippine Sea Plate in the northeast, and the Sorong Fault, which exhibits strike-slip motion in the southern part of the island (see Fig. 1). This tectonic process results in the creation of a multifaceted geological formation and governs the evolution of geological characteristics (Fig. 2). The geological framework of Halmahera Island comprises many components, including arc fragments, a microcontinent, and an oceanic sea floor basin (van Bemmelen, 1949; Hall and Spakman, 2015; Konopka et al., 2022). Halmahera's geological configuration began through the convergence process involving the eastern portion of the Molucca Sea Plate (Hall, 1987).

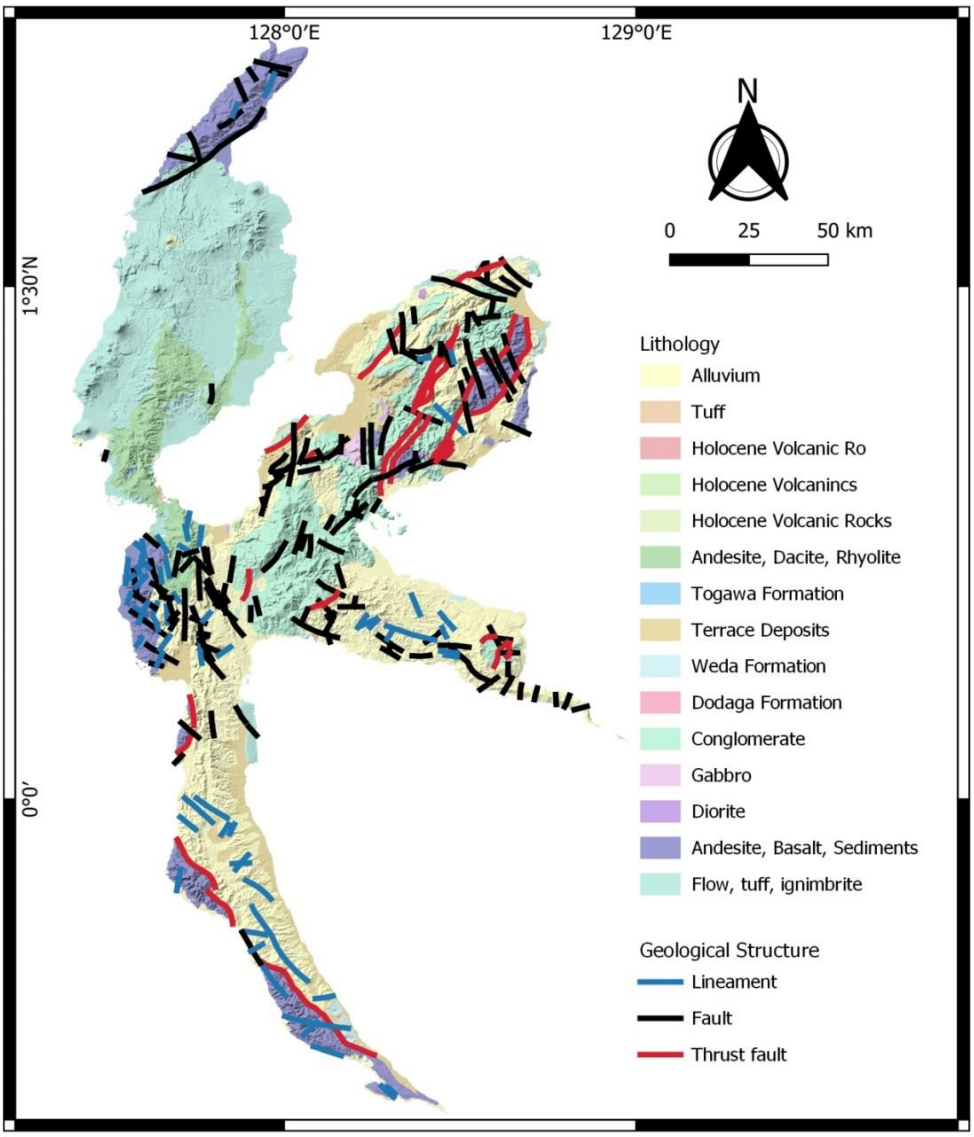

Figure 2. Regional geological map of Halmahera Island (modification from Sukamto and Samodra, 1995)

The process described involves the occurrence of subduction beneath the Halmahera region, wherein the Halmahera Plate actively consumes the Molucca Sea Plate. The ophiolite rocks under consideration are the result of subduction processes, followed by their subsequent uplift due to the collision between the Halmahera Plate and the Eurasian Plate above the Molucca Sea Plate (Cardwell and Karig, 1980; Mccaffrey et al., 1980; Hall and Hidayat, 1988; Hall et al., 1995; Milsom, 2001; Hinschberger et al., 2005; Dong et al., 2022). The collision event results in the formation of a volcanic arc before the tertiary period, characterized by ongoing volcanic activities and volcaniclastic rock that overlies the ophiolite basement in the western region of Halmahera. This information is depicted in Fig. 2, as referenced by Hall and Wilson (2000), Waltham et al. (2008), Dang (2015), and Bani et al. (2021).

The westward motion of the Philippine Sea Plate resulted in three instances of subduction. One of these events involved the Eurasian Plate and led to a strike-slip movement along the Philippine Fault in the northeastern region (Hamilton, 1979; Waltham et al., 2008) (see Fig. 1). The formation of the Philippine Trench can be attributed to the subduction of the Philippine Sea Plate beneath the Eurasian Plate, as well as the subduction of the lithosphere of the Molucca Sea Plate beneath the Philippine Sea Plate in the western region, namely below Halmahera. This explanation is supported by studies conducted by Silver and Moore in 1978, Zhang et al. in 2017, and Rachman et al. in 2022. The primary geological feature of the eastern portion of Halmahera is a Mélange Complex, which has formed due to deformation on the underlying ophiolite basement (Hamilton, 1979; van Gorsel, 2018; Konopka et al., 2022). The strike-slip on the eastern Halmahera arm can be attributed to the continued movement of the Philippine Sea Plate, as noted by Silver and Moore (1978). This observation is further corroborated by the seismic activity reported in this region by Hall (1987). Several stages of geological structure development are in the southern arm of Halmahera. It begins with the tectonism of the Sorong Fault, causing the basement to be deformed (Hall et al., 1991). Metamorphism accompanied the deformation of the lithology surrounding the area. This deformation pressed the contact block of the major fault, followed by intensive folding with the local over-thrusting positioned in the junction of the west arc and the east back-arc region. It uplifted and ended up by erosion.

3. Data

This research utilizes two satellite data. The first dataset uses GGMplus gravity satellite data by Hirt et al. (2013), and the second uses satellite data as sentinel 1-A. The satellite gravity data has proven to be an effective method for characterizing subsurface structures, as demonstrated by studies conducted by Nigussie et al. (2022) and Alrefaee et al. (2022). This approach is particularly advantageous when dealing with extensive regions that present difficulties in terms of accessibility, whether they are located on land or in marine environments. The gravity data utilized in this investigation were acquired from GGMPlus, a dataset developed by Hirt et al. (2013), which offers information on the acceleration caused by gravity. The dataset can be downloaded at the following website: https://murray-lab.caltech.edu/GGMplus/index.html. The GGMPlus model integrates multiple elements, including the GOCE/GRACE satellite gravity data, the Earth gravity model (EGM2008), and topographical gravity derived from the SRTM topography as outlined in the works of Hirt et al. (2013) and Hirt et al. (2014).

Furthermore, the acquisition of elevation data was facilitated by using imagery from the

Shuttle Radar Topography Mission (SRTM), sourced from the official website of the United States Geological Survey (USGS) at https://usgs.gov. In addition, remote sensing data was acquired from the Sentinel-1A satellite and analyzed using the Single-Look Complex (SLC) technique, which accounts for slant distance geometry, phase preservation, and natural pixel spacing. The raw data of Sentinel-1A was obtained by downloading it from the Alaska Satellite Facility (ASF) official website at https://search.asf.alaska.edu/.

4. Methods

4.1. Remote sensing

The Synthetic Aperture Radar (SAR) Sentinel-1A uses advanced remote sensing technology to overcome the limitations of optical imagery, such as the ability to penetrate clouds and vegetation cover (Dhara et al., 2022; Dai et al., 2023). Sentinel-1A adopts the C-band, offering spatial resolutions of 5 × 5, 5 × 20, or 20 × 40, with a wavelength ranging from 3.75 to 7.5 cm (Ahmadi and Pekkan, 2021). SAR works without the sun's electromagnetic waves because it uses an active source (Li et al., 2022; Zhao et al., 2023). This allows for effective operation and the collection of surface information. In addition, the signal's wavelength is powerful in detecting the physical properties of materials on the surface. Moreover, the applications of SAR imagery extend to lineament delineation.

The Yamaguchi method focuses on two factors to recognize geological features: image scale and orbit. A smaller scale is more efficient for observing lineaments over larger areas, but it may reduce the image quality. Conversely, employing a larger scale yields more excellent reliability in examining characteristics within the localized data. To investigate this matter, Yamaguchi (1985) defines the relationship between resolution and image scale as written in the Equation below:

$$R \times S = 0.1\,mm \quad (1)$$

where R is the resolution and S is the scale of the remote sensing data.

4.2. Gravity

The utilization of gravity anomalies, vertical derivatives, and the integration of gravity anomalies with horizontal derivatives has demonstrated that it is successful in the identification of edges and determination of depths within the subsurface rock formations. In a recent study, the derivative technique of gravity data has been reported to enhance the sharpness of discontinuity boundaries beneath the surface, as documented by Oksum et al. (2021), Altinoğlu (2023), Alvandi et al. (2023), Kamto et al. (2023), and Pham et al. (2023). The utilization of derivatives is well-known in the context of edge detection filters. One such filter employed in this research is the fast sigmoid edge detection (FSED). FSED is the ratio of the first derivatives of the gradient amplitude. This approach demonstrates a maximum response over the edge of the anomaly source (Oksum et al., 2021; Alvandi et al., 2023).

This filter can balance anomalies originating from various depths by tilizing the vertical and horizontal derivatives of gravity gradient data. The proposed FSED Equation by Oksum et al. (2021) is illustrated in Equation (2):

$$FSED = \frac{R-1}{1+|R|} \quad (2)$$

with

$$R = \frac{\frac{\partial THG}{\partial z}}{\sqrt{\left(\frac{\partial THG}{\partial x}\right)^2 + \left(\frac{\partial THG}{\partial y}\right)^2}} \quad (3)$$

where $\partial THG/\partial z$ is the vertical derivative of total horizontal gradient ∂THG, $\partial THG/\partial x$ and $\partial THG/\partial y$ denote the horizontal derivative of total horizontal gradient in the x

and y directions, respectively. The FSED effectively mitigates amplitude anomalies arising from causative bodies at varying depths and with distinct properties, enhancing resolution and accuracy in delineating source edges. Notably, this filter avoids generating spurious edges in cases where anomaly sources exhibit opposing density contrasts simultaneously, as demonstrated by Oksum et al. (2021), Eldosouky et al. (2022), Kamto et al. (2023), and Pham et al. (2023).

$$(x - x_0)\frac{\partial^2 f}{\partial z \partial x} + (y - y_0)\frac{\partial^2 f}{\partial z \partial y} + (z - z_0)\frac{\partial^2 f}{\partial z^2} = N\frac{\partial f}{\partial z} \quad (4)$$

f denotes the gravity field at the point of x, y, z affected by the anomaly source at x_0, y_0, z_0 position. In this study, the parameter N, where N is defined as the sum of the structural index (SI) and the vertical gradient order of the gravity data (n), represents the structural index that characterizes the geometric parameters of the source (Huang et al., 1995; Cooper, 2004; Stavrev and Reid, 2007; Pham et al., 2023). In the gravity case, SI = -1 represents lithological contact or fault, 0 for a thin sheet, 1 is used for a horizontal cylinder, and 2 is a geometric sphere (Reid and Thurston, 2014; Abdullahi et al., 2023).

5. Data processing

5.1. Imagery Pre-processing based on remote sensing approach

The Synthetic Aperture Radar (SAR) data were obtained under dry conditions on April 4, 2017, utilizing ascending and descending orbits and dual polarization. The dataset of Sentinel-1A imagery encompasses a considerable geographical extent, hence requiring the segmentation (TOPSAR-Split) of segments to extract imagery relevant to the study area and mitigate the inclusion of extraneous pixel data. The data is subjected to radiometric correction to mitigate the presence of speckles. Using the Sentinel Applications Platform (SNAP) software facilitates the alignment of pixels to their corresponding actual positions, hence mitigating the perceptibility of layover, shadow, and foreshortening effects (Gyeltshen et al., 2022). Lineament extraction is performed on the geometrically corrected SAR imagery at a scale of 1:280.000.

In addition to FSED technique, depth information is acquired through the Euler deconvolution method. The Euler deconvolution method was first employed to determine the positions of lineament in magnetic data (Thompson, 1982; Reid et al., 1990; Cooper, 2004; Pham et al., 2023). Marson and Klingele (1993) endeavor to employ the Euler approach, as elucidated by Pham et al. (2023). The Equation of Euler is formulated as seen below:

5.2. Anomaly separation and enhancement data using gravity method

The data obtained from the GGMPlus satellite remains in the form of gravity acceleration. Hinze et al. (2013) employed a methodological approach using various theoretical gravity corrections, namely latitude, free-air, terrain, and Bouguer gravity corrections, to obtain complete Bouguer anomaly (CBA) values. The present study utilizes the Kriging interpolation technique to create CBA data on a 220 × 220 m grid. Two processing stages have been applied to the CBA data: anomaly separation and edge detection. Generally, short wavelengths represent residual anomalies and noise, while long wavelengths are associated with regional anomalies (Abdelrahman et al., 1985). This research uses bandpass filters to separate the residual from the CBA.

Implementing the FSED data enhancement method involves the CBA map as input data, followed by horizontal and vertical gradient component computation through the

numerical derivative technique in the frequency domain. The delineation of subsurface source edges is performed at the maximum value of FSED, representing formation boundaries and geological structure (Oksum et al., 2021; Eldosouky et al., 2022; Pham et al., 2023; and Kamto et al., 2023). The rock body boundaries are drawn using the FSED method, supported by research established by Oksum et al. (2021), Pham et al. (2023), and Kamto et al. (2023). In addition to FSED, Euler edge detection is further practiced in this study to approximate the depth of anomalies. This study applies Euler deconvolution with an N of 0 derived from Equation 3 using SI = -1 and n = 1.

Additionally, several studies' proposed window size parameter is 10 × 10 km, as mentioned in Castro et al. (2020) and Pham et al. (2023). Here, we applied the Euler deconvolution method by assuming a contact model with a 10 × 10 moving window to locate possible subsurface structures from gravity data.

6. Results

6.1. Lineament analysis using Sentinel-1A imagery

The geological feature, specifically the lineament identification, was analyzed by combining two scenes, the ascending and descending imagery. A total of 6203 lineaments were discovered throughout the entire Halmahera Island. The lineament map interpretation considered three factors: the dominant strike direction of the lineaments the continuous lineaments' avoidance of radial volcanic trends. Lineaments were delineated in each arm of Halmahera Island, including the northern arm (Fig. 3), the northeastern arm as illustrated in Fig. 4, the central arm (Fig. 5), and the southern arm, which can be seen in Fig. 6.

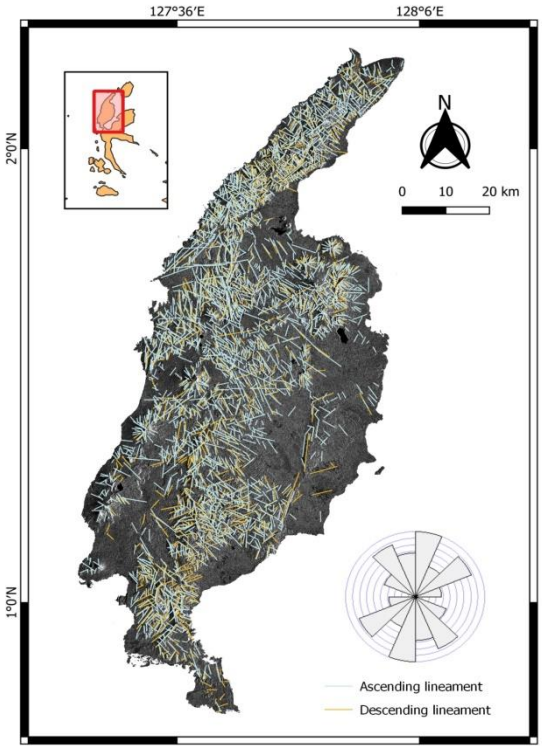

Figure 3. Lineament analysis of Sentinel-1A dual orbit ascending (blue line) and descending (orange line) imagery on the northern arm of Halmahera

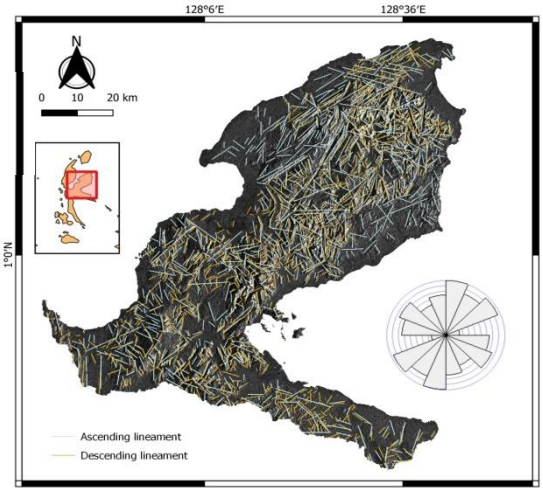

Figure 4. Lineament analysis of Sentinel-1A dual orbit ascending (blue line) and descending (orange line) imagery on the northeastern arm of Halmahera

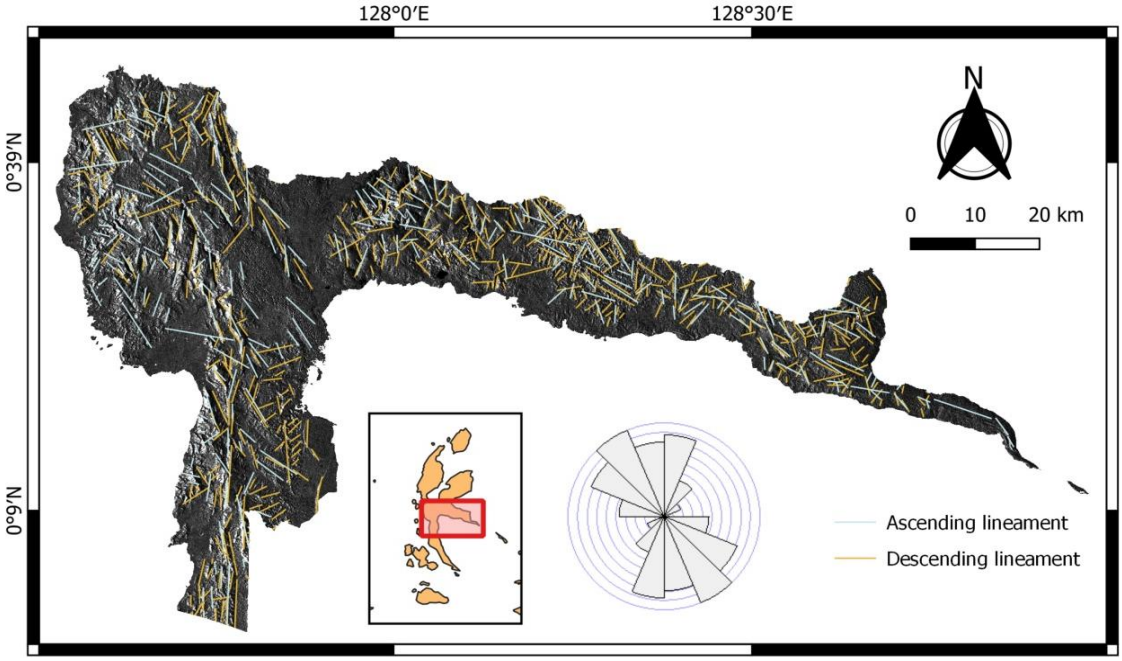

Figure 5. Lineament analysis of Sentinel-1A dual orbit ascending (blue line) and descending (orange line) imagery on the central arm of Halmahera

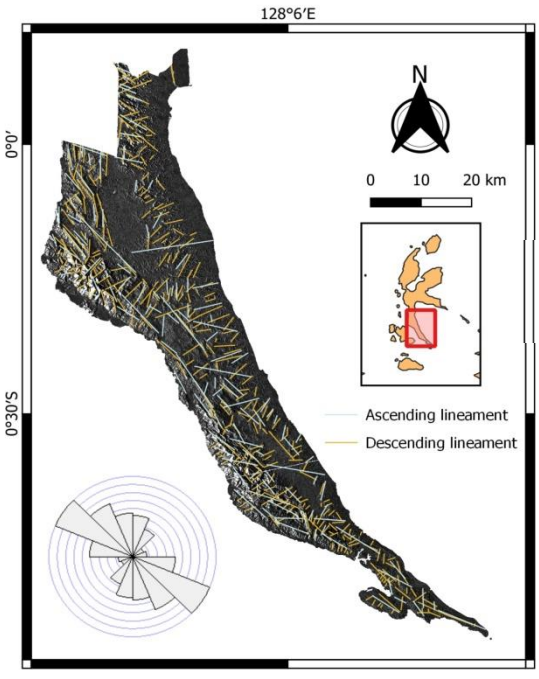

Figure 6. Lineament analysis of Sentinel-1A dual orbit ascending (blue line) and descending (orange line) imagery on the southern arm of Halmahera

6.2. Gravity anomaly

The Complete Bouguer Anomaly (CBA) shows regional variations, with positive values ranging from 67 to 220 mGal, as depicted in Fig. 7. The gravity anomalies seen in the northern arm have a comparatively greater magnitude of 220 mGal, in contrast to the southern volcanic arc where the anomalies measure 143 mGal. This discrepancy suggests that the northern area possesses elevated topography characterized by the presence of materials with higher density. Conversely, diminished gravitational anomalies within the volcanic arc indicate a relatively lower density of rocks compared to the surrounding areas. The complicated geological events on Halmahera have led to an intricate distribution of rocks and subsurface structures, resulting in a very varied gravity field response (Fig. 7).

The depth estimation uses the Radially Averaged Power Spectrum (RAPS) adopted

from Spector and Grant (1970). The average power spectrum's slope represents the discontinuity depth between two different anomalous sources. The part of the curve with the lowest wavenumber value (cycle/km) from 0 to 0.05 represents a deep anomalous source. In contrast, wavenumbers greater than 0.5 are interpreted as signals from shallow anomalies that could be noise. Wavenumbers values in the range of 0.05 to 0.5 are considered to be anomalous sources represented by rocks near the surface.

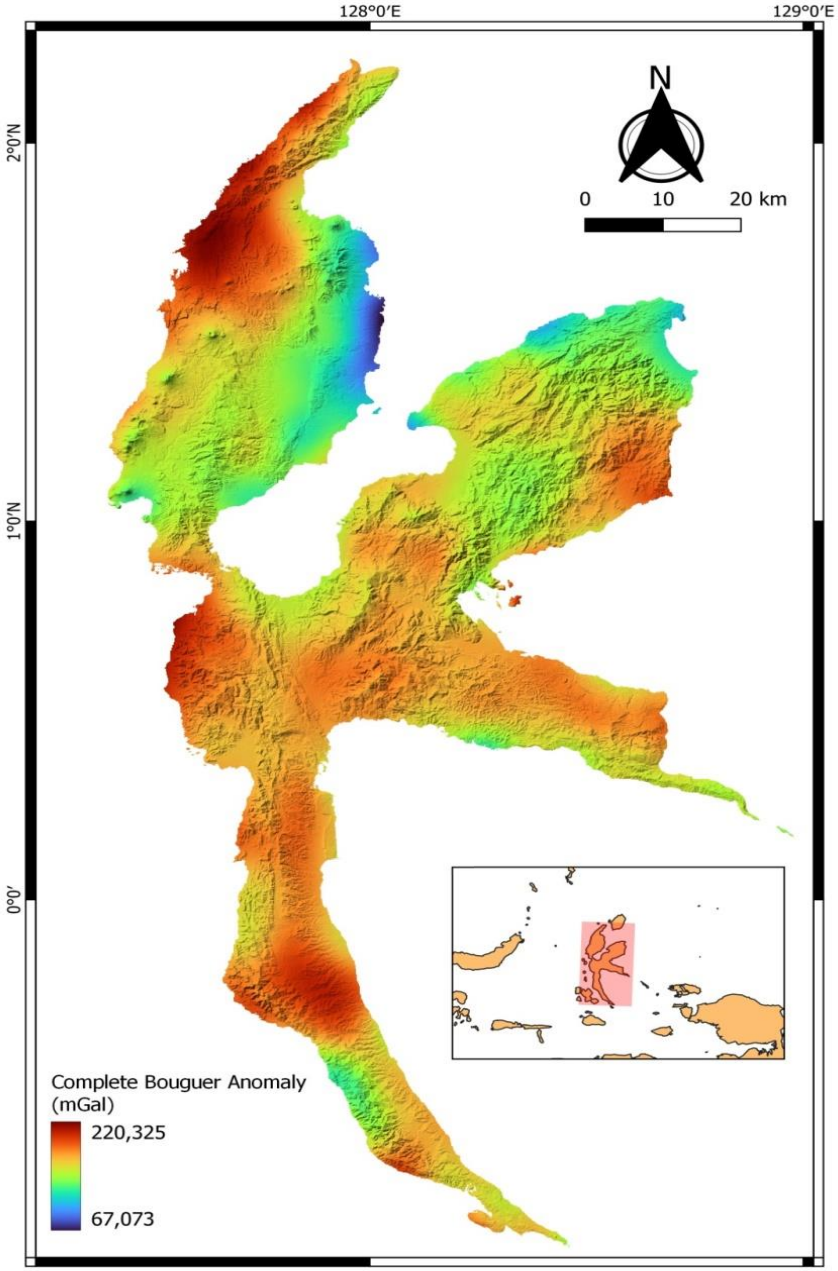

Figure 7. Complete Bouguer Anomaly (CBA) of study area

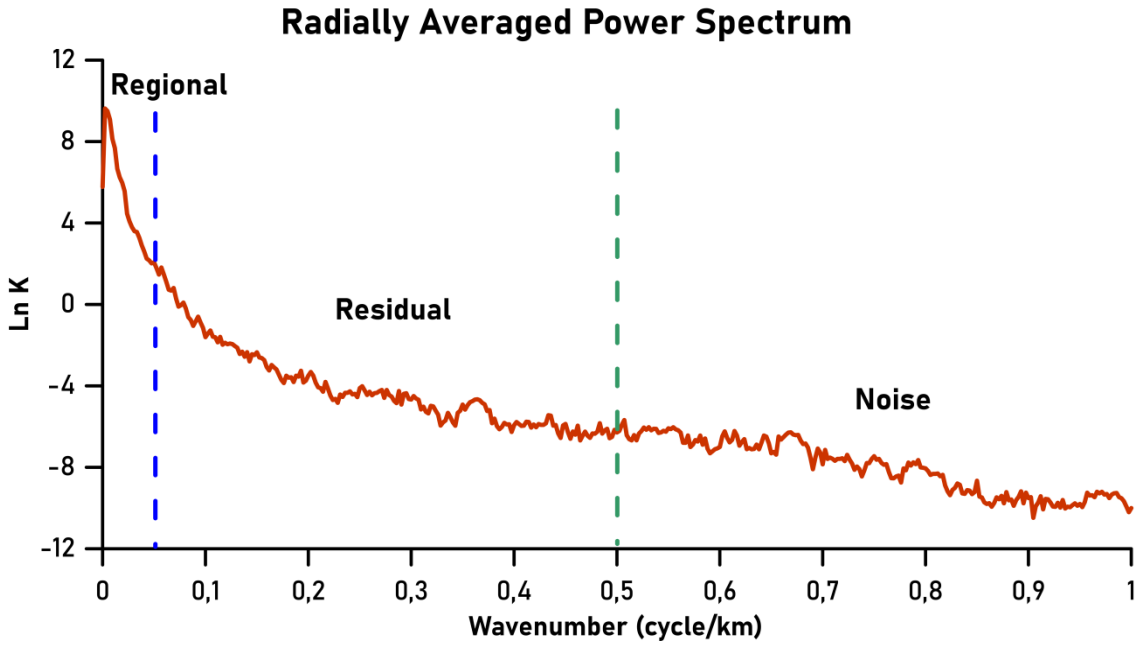

Figure 8. Cut-off frequency in regional and residual gravity anomaly with Radially Averaged Power Spectrum (RAPS)

The depth segment boundaries of this anomalous source are shown in Fig. 8. After the process of anomaly separation, the resulting residual gravity anomaly displays a variation between -6.651 and 6.42 mGal. This observation indicates the presence of shallow geological features, specifically residual anomalies, as seen in Fig. 9. Moreover, the geological characteristics are augmented by the presence of FSED, which varies from -1 to 1, as illustrated in Figs. 10a-13a. The estimated depths, derived from Euler deconvolution (Figs. 10b-13b), shown by dot plots with color variations representing the different depths, indicate that these features extend up to 5000 meters below the surface. The FSED solution technique shows the interpretation of the geological structure at the boundary where the value is maximum (Oksum et al., 2021; Pham et al., 2023). The Euler depth analysis identifies the location of geological features, such as formation boundaries or faults, using the lineament estimation represented by the yellow line.

Regarding each arm of Halmahera Island, these two analyses reveal an identical dominant trend (Figs. 10-13). This visualization contributes to enhancing the understanding of the geological features. In these results, implementing the FSED technique has proven effective in interpreting causative body boundaries by balancing the anomalous response contributions from deep and shallow structures.

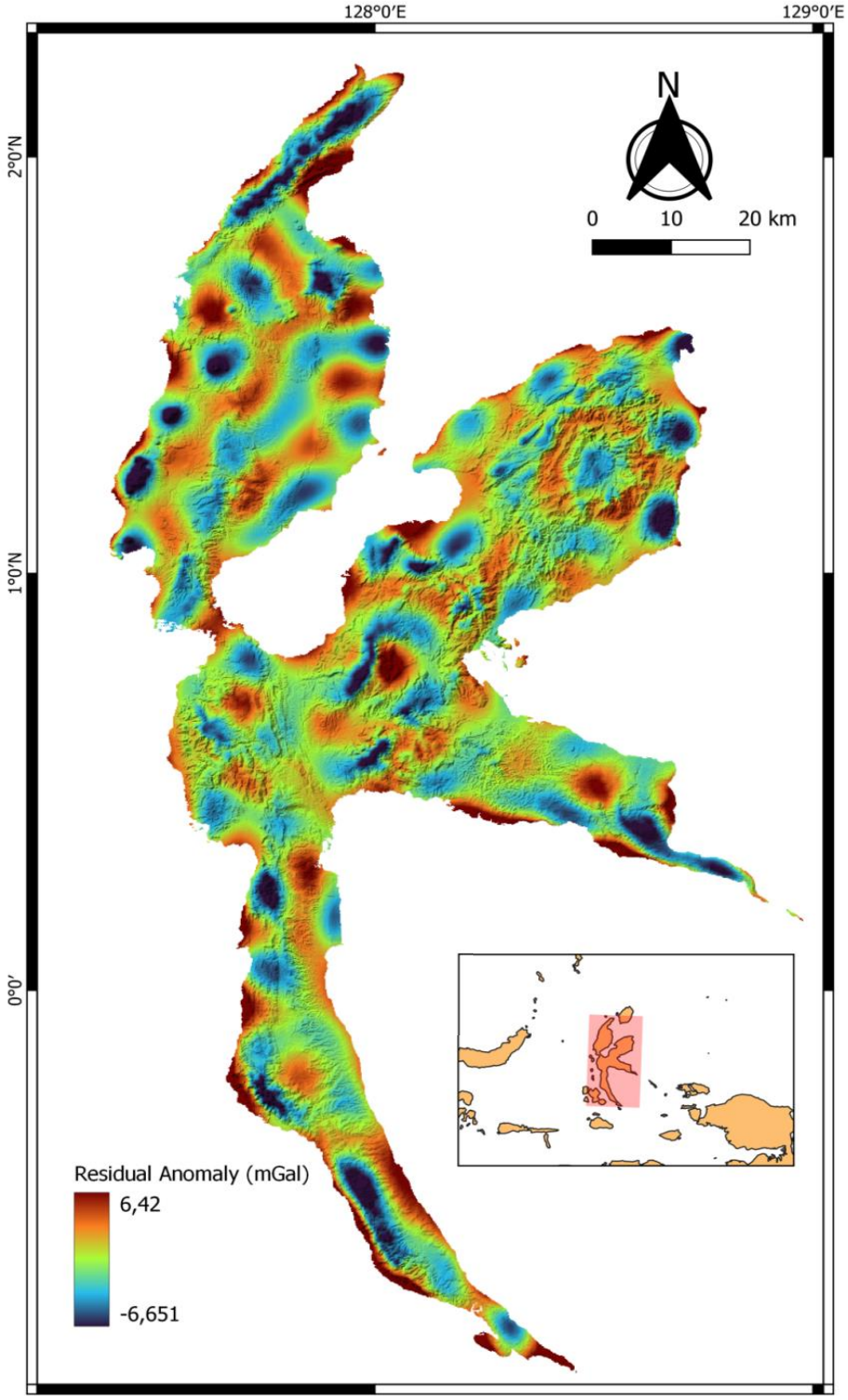

Figure 9. Residual anomaly map for Halmahera region

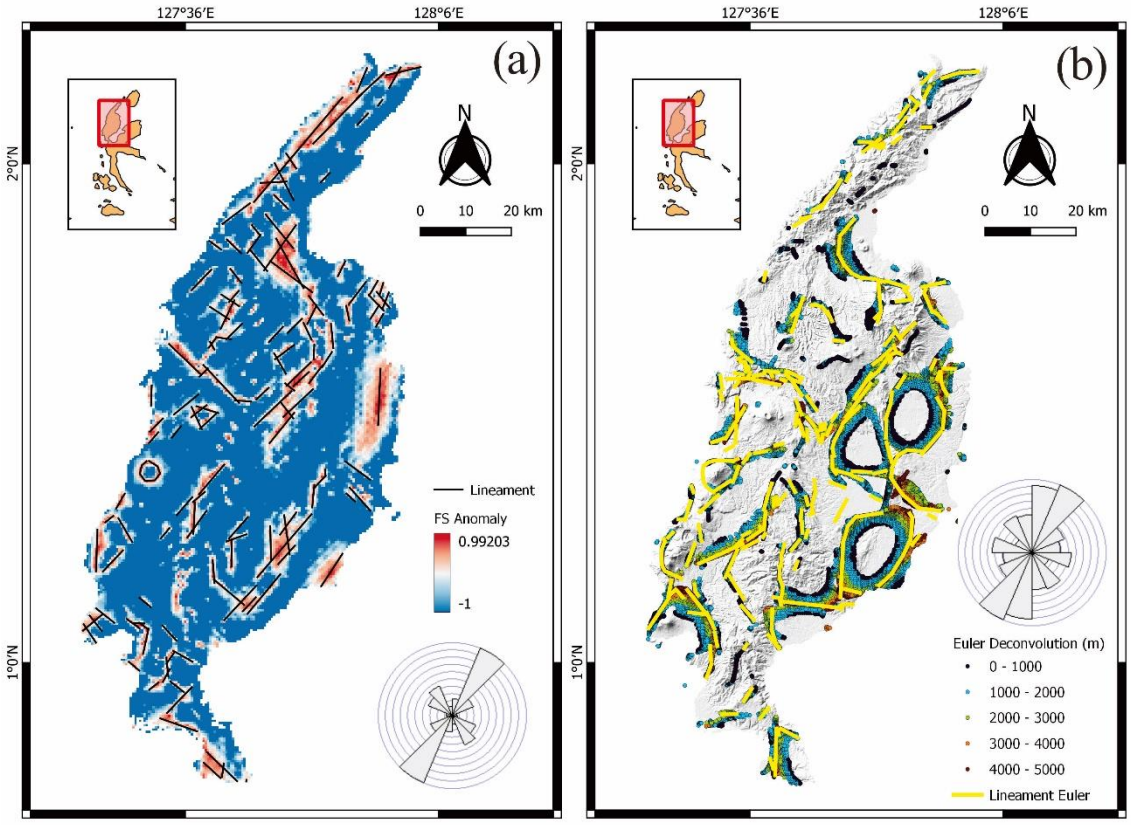

Figure 10. Lineament extraction on gravity data is based on the application of edge detection techniques on the northern Halmahera arm (a) FSED, (b) Euler deconvolution. The black solid line shows structural delineation in FSED, while the yellow solid line shows structural delineation in Euler depth estimation

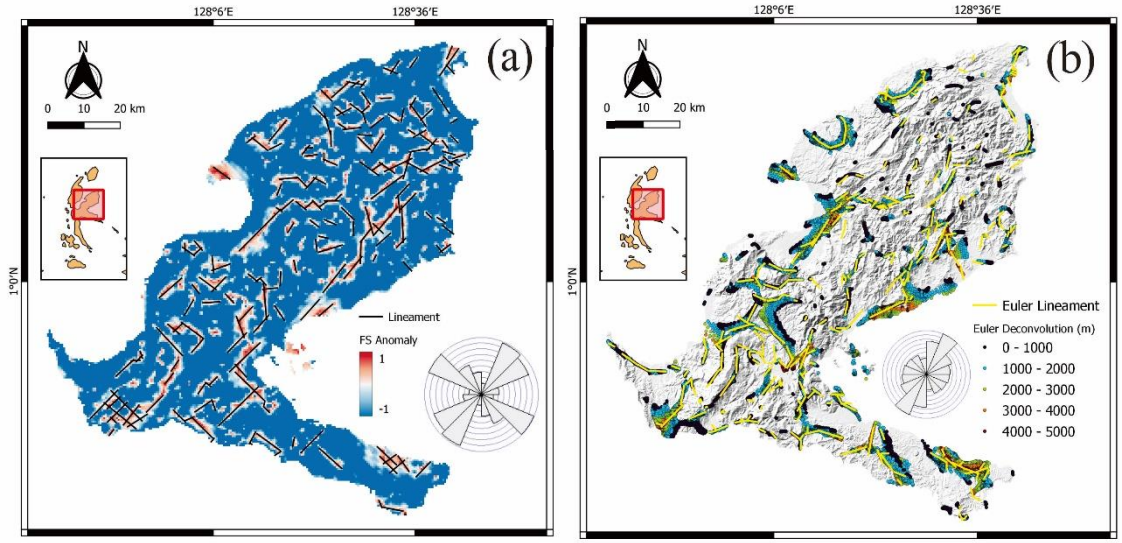

Figure 11. Lineament extraction on gravity data is based on the application of edge detection techniques on the northeastern Halmahera arm (a) FSED, (b) Euler deconvolution

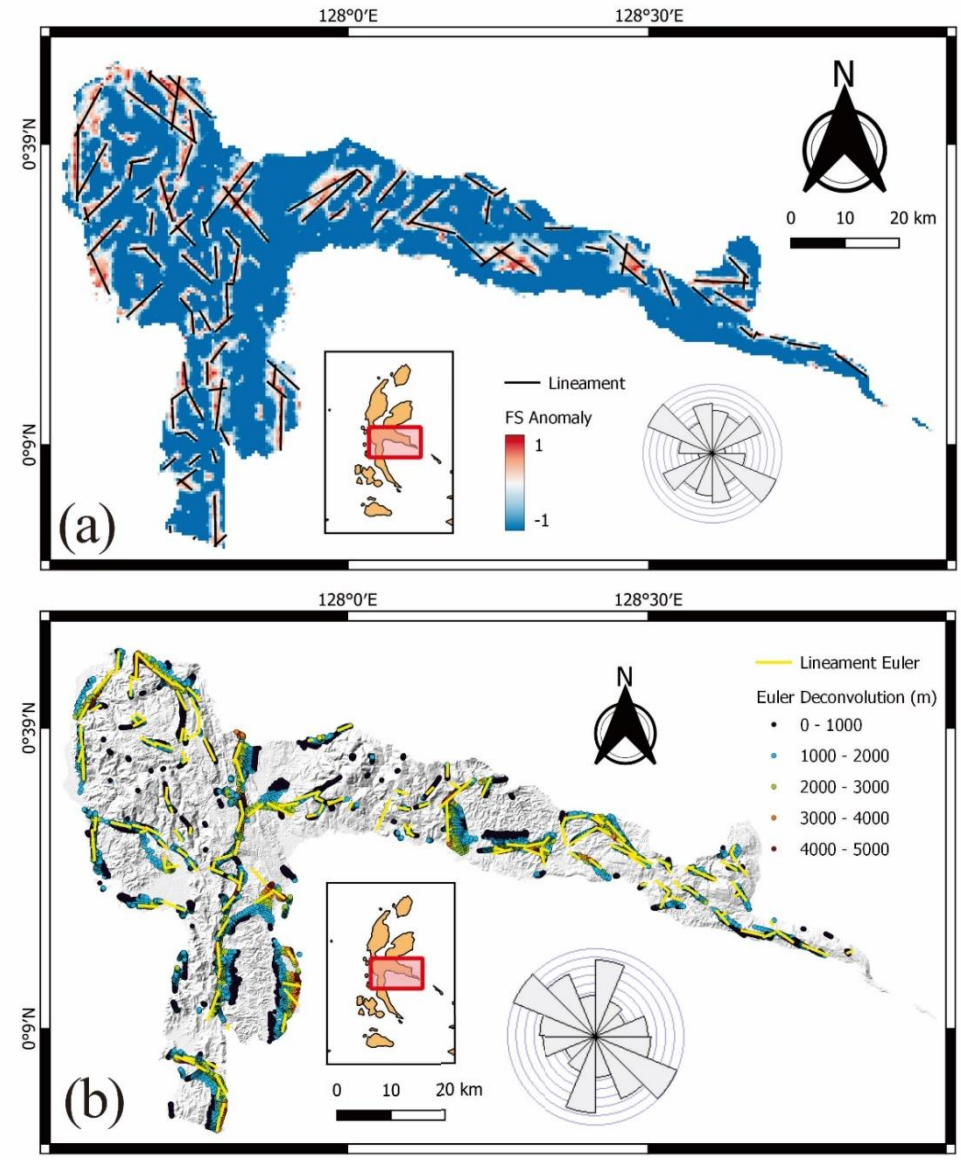

Figure 12. Lineament extraction on gravity data is based on the application of edge detection techniques on the central Halmahera arm (a) FSED, (b) Euler deconvolution

7. Discussions

7.1. Lineament analysis using the remote sensing method

Remote sensing analysis is obtained to determine the trend of structures near the surface. The structural analysis was carried out with a Rose diagram. The findings of the investigation of this methodology are depicted in Figs. 3 to 6. The northern arm, as depicted in Fig. 3, is dominated by a volcanic arc extending in a NE-SW direction. This volcanic arc is the product of volcanic magmatism resulting from the collision between the Molucca Sea Plate and the Halmahera Plate. This collision plays a significant role in forming the structural history of the area. This structure with an NE-

SW orientation is associated with the subduction of the Pacific microcontinent beneath the Eurasian Plate. In the northeastern arm of Halmahera (Fig. 4), the NE-SW trend is formed by a complex geological context caused by tectonic processes. In addition, the geological structure that develops on the southern arm of Halmahera Island is affected by the strike-slip motion of the Sorong Fault as a result of the release of collision energy between the Indo-Australian Plate and the Pacific Plate to the north and west, respectively. Compared to the other arms, the central Halmahera arm (Fig.5) has two predominant trends, namely NW-SE and NE-SW directions, whereas the southern arm (Fig. 6) has an NW-SE trend.

7.2. Application of edge detection technique and euler dpth estimation

The gravity anomaly has been spatially analyzed and interpreted to understand regional structural trends in the Halmahera region. The FSED technique analysis of each Halmahera arm supports the results of this study. The northern arm is illustrated in Fig. 10a, the northern-northeastern arm in Fig. 11a, the central arm in Fig. 12a, and the south arm in Fig. 13a. The Euler depth solution defines the estimated depth of the anomaly source based on the vertical gravity data derivative derived using the Euler deconvolution method (Marson and Klingele, 1993; Pham et al., 2023). Figs. 10b–13b shows each arm's Euler depth estimation evaluation. The results of the analysis of the FSED technique generate sharp responses over the boundaries of anomalous sources. Furthermore, Euler's technique displays more detailed lineament trends of geological structures represented by each source depth. The Euler technique can identify lateral and vertical anomaly source boundaries simultaneously to provide the results of structural continuity with depth.

The geological structure of the Halmahera area is thought to be a source of deep structures, reaching more than 4 km, while shallow structures are at depths of up to 2 km. It has been suggested that all Halmahera arms are closely related to shallow structures (Figs. 10b-13b). However, the Euler deconvolution method on all arms still generates an imprecise solution due to several factors, such as noise and interference from surrounding anomalies (Chen et al., 2014).

The utilization of the FSED approach and Euler depth solution revealed that the boundary of the anomaly exhibited consistent characteristics, providing geological insights into the spatial limits of the anomaly's source on Halmahera Island. The black solid line represents the structural delineation from the FSED approach, while the yellow solid line corresponds to the Euler depth solution. The Euler depth solution estimates the location of geological features, such as formation boundaries or faults, between different volcanic rocks and the Mélange Complex in the region (Sukamto and Samodra, 1995). The dipping contact at the same source depth determines the delineation of the geological structure's boundaries. As a result, the lineament of the boundary structure is established with an NE-SW trend on the northern (Fig. 10) and northeastern arms (Fig. 11). Conversely, the southern arm exhibits a predominant direction that is opposite to the northern and northeastern arm, explicitly following an NW-SE trend (Fig. 13). The minor structural trends seen in the northeastern arm (Fig. 11), known as the N-E and E-W trends, are believed to have originated from compression folding. These folding events are thought to be associated with the migration of the Philippine microcontinent, which involved the occurrence of shear faults along the Mélange Complex. This interpretation is supported by previous studies conducted by Hall (1987), Sukamto, and Samodra (1995).

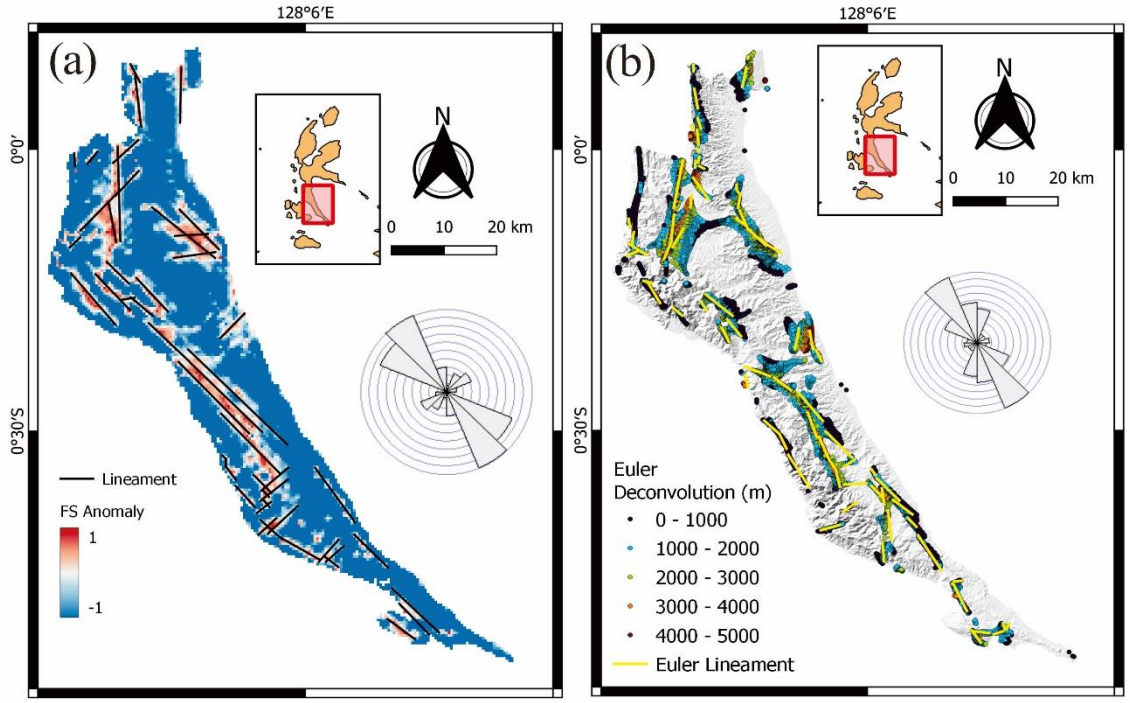

Figure 13. Lineament extraction on gravity data is based on the application of edge detection techniques on the southern Halmahera arm (a) FSED, (b) Euler deconvolution

The structure in the central arm exhibits two dominant intersecting trends (Fig. 12): NW-SE and NE-SW. These lineaments of interpreted structures are discernible through the implementation of the FSED edge detection (Fig. 12a) and Euler deconvolution (Fig. 12b). The distribution trends of these lineaments, along with their respective orientations, exhibit a correlated relationship as indicated by the rose diagrams on both maps. Lineaments trending NW-SE display a tendency towards strike-slip faulting, substantiated by findings from Hall et al. (1991). Conversely, indications suggest dip-slip fault for the orientation of the other dominant lineament. This finding is consistent with Sukamto and Samodra (1995) trend analysis of regional structure (Fig. 2). On the southern arm of Halmahera, the anomaly boundary trends display a northwest-southeast (NW-SE) orientation. This suggests a continuance or extension of the geological structure (Hamilton, 1979; Hall, 1987; Hall and Hidayat, 1988; van Gorsel, 2018)

7.3. Structural of Halmahera

Integrating geological structure lineaments from gravity anomaly data with remote sensing analysis yields comprehensive outcomes related to the structural trends that formed on Halmahera Island. The findings from both approaches exhibit an identical trend. Tectonic seismicity data is needed to support interpreting gravity data and remote sensing in delineating geological structures. The compatibility of the geological structure's lineament with the hypocentre of the earthquake is evident from the plotted positions of both entities (Figs. 14a–d). The geological conditions of Halmahera Island are shown to be mutually validated through interpretations derived from gravity and remote sensing techniques. The integration of the two techniques

indicates that the northern region of Halmahera Island has a structural lineament that has not been documented previously. The complex structure of the geological formation in the northern arm is believed to have a strong correlation with the Halmahera Trench and the Philippine Trench (Hall and Spakman, 2015; van Gorsel, 2018).

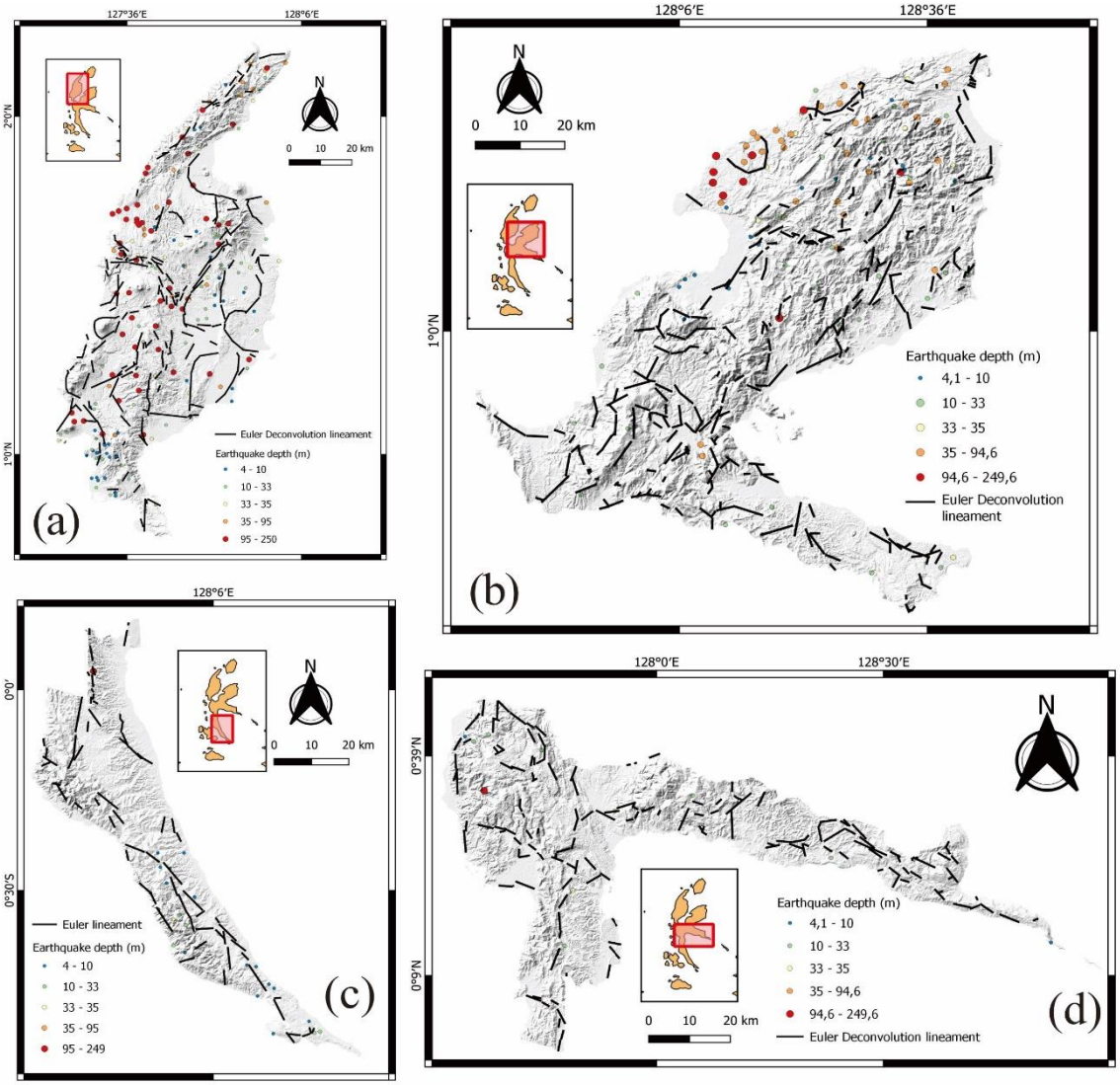

Figure 14. Lineament extraction from the Euler method and hypocenter plots of earthquakes of Halmahera (a) North arm, (b) Northeast arm, (c) South arm, (d) Central arm

The movement of the Philippine Sea Plate to the west and the Sorong Fault with a rotational movement suppresses the southern part, forming a NE-SW strike-slip movement in the north (Fig. 3, Fig. 10). This is supported by Hall (1987) assertion of the existence of a NE-SW fault that crosses between the northern and northeastern arms. Finally, the interpretation of the geological structure trend in the northern and northeastern arms of the island (Fig. 3, Fig. 4, Fig. 10, Fig. 11) contrasts with the geological structure trend in

the southern part of the island (Fig. 6, Fig. 13) because the southern part of the island is still strongly controlled by the Sorong Fault (Hall, 1987; van Gorsel, 2018; Patria et al., 2021). Meanwhile, in the central arm (Fig. 5, Fig. 12), the structure is actively controlled by Halmahera's subduction and the Philippine Sea Plate's rotational movement (Hall, 1987).

There are distinctions between the outcomes of these two interpretations. It is believed that Halmahera Island is controlled by two distinct tectonic processes: (1) the southern part has a strike-slip fault due to the northwest-southeast trending Sorong Fault, and (2) the northern part is controlled by the subduction zone of the Halmahera Plate and the Molucca Sea Plate, as well as the strike-slip, which is the accommodation of the Sorong Fault and the Philippine Trench.

8. Conclusions

The lineament delineation based on remote sensing imagery of Halmahera shows a dominant trend in the NE-SW direction on the northern and northeastern arms, while the south arm is NW-SE. The central arm has a trend in two directions, NE-SW and NW-SE, which are combined trends of the northern and southern arms. Also, identifying structures in the Halmahera area based on the gravity response from both FSED analysis and Euler depth estimation gives an idea of structures that can't be seen from the surface. Interesting geological interpretations seen in the north have geological structure trends that have not been mapped before. The dominant structure of Halmahera Island in the northern arm trending NE-SW is associated with the Philippine Sea microcontinent that collides with the Halmahera Plate. The integration of these two methods confirms and provides new information that the southern part has a strike-slip fault due to the Sorong Fault, which is trending NW-SE, and the northern part is dominated by the rotational movement of the southern Philippine Sea microcontinent, which is subducting beneath the Halmahera Plate. Based on the results obtained from the analysis of the gravity method, it correlates well with the remote sensing method in delineating the regional geological lineament of Halmahera Island, North Molucca.

Acknowledgements

The authors thank the Faculty of Mining and Petroleum Engineering and the School of Graduate Studies of Institut Teknologi Bandung for their administrative support. Also, the authors would like to thank the International Gravimetric Bureau for providing freely accessible gravity data (http://ddfe.curtin.edu.au/gravitymodels/GGMplus/data/).

References

Abdelrahman E.M., Riad S., Refai E. M., Amin Y., 1985. On the least-squares residual anomaly determination. Geophysics, 50(3), 473–480.

Abdullahi M., Kumar R., Idi B.Y., Singh U.K., Abba A.U., 2023. Analysis of recent airborne gravity and magnetic data for the interpretation of basement structures underneath the south western Benue trough using source edge detector filters. Acta Geophysica, 71, 1595–1606.

Ahmadi H., Pekkan E., 2021. Fault-based geological lineaments extraction using remote sensing and GIS a review. Geosciences (Switzerland), 11(5), 1–31.

Alrefaee H.A., Soliman M.R., Merghelani T.A., 2022. Interpretation of the subsurface tectonic setting of the Natrun Basin, north Western Desert, Egypt using Satellite Bouguer gravity and magnetic data. Journal of African Earth Sciences, 187(104450), 1–16.

Altinoğlu F.F., 2023. Mapping of the structural lineaments and sedimentary basement relief using gravity data to guide mineral exploration in the Denizli Basin. Minerals, 13(10), 1276.

Alvandi A., Su K., Ai H., Ardestani V.E., Lyu C., 2023. Enhancement of potential field source boundaries using the hyperbolic domain (gudermannian function). Minerals, 13(10), 1312.

Bani P., Nauret F., Oppenheimer C., Aiuppa A., Saing B.U., Haerani N., Al H., Marlia M., Tsanev V.,

2021. Heterogeneity of volatile sources along the Halmahera arc, Indonesia. Journal of Volcanology and Geothermal Research, 418(107342), 1−12.

Bird P., 2003. An updated digital model of plate boundaries. Geochemistry, Geophysics, Geosystems, 4(3), 1−52.

Cardwell R.K., Karig D.E., 1980. The spatial distribution of earthquakes, focal mechanism solutions, and subducted lithosphere in the Philippine and Northeastern Indonesian Islands. Submar. Landslides, 23, 1-35.

Castro F., Oliveira S.P., de Souza J., Ferreira F.J.F., 2020. Constraining Euler deconvolution solutions through combined tilt derivative filters. Pure and Applied Geophysics, 170, 4883−4895.

Chen Q., Dong Y., Cheng S., Han L., Xu H., Chen H., 2014. Interpretation of fault system in the Tana Sag, Kenya, using edge recognition techniques and Euler deconvolution. Applied Geophysics, 109, 150−161.

Chen Q., Dong Y., Tan X., Yan S., Chen H., Wang J., Wang J., Huang Z., Xu H., 2022. Application of extended tilt angle and its 3D Euler deconvolution to gravity data from the Longmenshan thrust belt and adjacent areas. Journal of Applied Geophysics, 206(104769), 1−3.

Cooper G.R.J., 2004. Euler deconvolution applied to potential field gradients. Geophysics, 35, 165−170.

Cooper G.R.J., Cowan D.R., 2006. Enhancing potential field data using filters based on the local phase. Computer & Geosciences, 32(10), 1585−1591.

Dai K., Chen C., Shi X., Wu M., Feng W., Xu Q., Liang R., Zhuo G., Li Z., 2023. Dynamic landslides susceptibility evaluation in Baihetan Dam area during extensive impoundment by integrating geological model and InSAR observations. International Journal of Applied Earth Observation and Geoinformation, 116(103157), 1−12.

Dang H., 2015. Precessional changes in the western equatorial Pacific Hydroclimate: A 240 kyr marine record from the Halmahera Sea, East Indonesia. Geochemistry, Geophysics, Geosystems, 16, 148−164.

Dhara M., Baisantry M., Prusty G., 2022. Automatic extraction and analysis of lineament features using ASTER and Sentinel 1 SAR data. Journal of Earth System Science, 131(2), 1−15.

Dong L., Luo Q., 2022. Investigations and new insights on earthquake mechanics from fault slip experiments. Earth-Science Reviews, 228(104019), 1−17.

Dong M., Zhang J., Jiang C., Hao T., Xu Y., Huang S., 2022. Thermal simulation of migration mechanism of the Halmahera volcanic arc, Indonesia. Journal of Asian Earth Sciences, 232(105042), 1−10.

Eldosouky A.M., Pham L.T., Henaish A., 2022. High precision structural mapping using edge filters of potential field and remote sensing data: A case study from Wadi Umm Ghalqa area, South Eastern Desert, Egypt. Egyptian Journal of Remote Sensing and Space Science, 25(2), 501−513.

Eldosouky A.M., Pham L.T., Mohmed H., Pradhan B., 2020. A comparative study of THG, AS, TA, theta, TDX and LTHG techniques for improving source boundaries detection of magnetic data using synthetic models: A case study from G. Um Monqul, North Eastern Desert, Egypt. Journal of African Earth Sciences, 170(103940), 1−9.

Elhag M., Alshamsi D., Agriculture A.L., Arabia S., Ain A., Dhabi A., Emirates U.A., 2019. Integration of remote sensing and geographic information systems for geological fault detection on the island of Crete, Greece. Geoscientific Instrumentation Methods and Data Systems, 8(1), 45−54.

Ghosh S., Sivasankar T., Anand G., 2021. Performance evaluation of multi-parametric synthetic aperture radar data for geological lineament extraction. International Journal of Remote Sensing, 42(7), 2574−2593.

Gyeltshen S., Kannaujiya S., Chhetri I.K., Chauhan P., 2022. Delineating groundwater potential zones using an integrated geospatial and geophysical approach in Phuentsholing, Bhutan. Acta Geophysica, 71(1), 341−357.

Haiyun W., Xiaxin T., 2003. Relationships between moment magnitude and fault parameters: theoretical and semi-empirical relationships. Earthquake Engineering and Engineering Vibration, 2(2), 201−211.

Hall R., 1987. Plate boundary evolution in the Halmahera region, Indonesia. Tectonophysics, 144(4), 337−352.

Hall R., Ali J.R., Anderson C.D., Baker S.J., 1995. Origin and motion history of the Philippine Sea Plate. Tectonophysics, 251(1−4), 229−250.

Hall R., Hidayat S., 1988. Basement rocks of the Halmahera region, eastern Indonesia: a late cretaceous-early tertiary arc and fore-arc. Journal of the Geological Society, 145, 65–84.

Hall R., Nichols G., Ballantyne P., Charlton T., Ali J., 1991. The character and significance of basement

rocks of the southern Molucca Sea region. Journal of Southeast Asian Earth Sciences, 6(3–4), 249–258.

Hall R., Spakman, W., 2015. Mantle structure and tectonic history of SE Asia. Tectonophysics, 658, 14–45.

Hall R., Wilson M.E.J., 2000. Neogene sutures in eastern Indonesia. Journal of Asian Earth Sciences, 18(6), 781–808.

Hamilton W., 1979. Tectonics of the Indonesian region. USGS Professional Paper, 1078.

Hinschberger F., Malod J., Réhault J., Villeneuve M., Royer J., Burhanuddin S., 2005. Late cenozoic geodynamic evolution of eastern Indonesia. Tectonophysics, 4040(1-2), 91–118.

Hinze W.J., Von Frese R.R.B., Saad A.H., 2013. Gravity and Magnetic Exploration: Principles, Practices and Applications. Cambridge University Press, New York, USA.

Hirt C., Claessens S., Fecher T., Kuhn M., Pail R., Rexer M., 2013. New ultrahigh-resolution picture of Earth's gravity field. Geophysical Research Letters, 40(16), 4279–4283.

Hirt C., Kuhn M., Claessens S.J., Pail R., Seitz K., Seitz K., Gruber T., 2014. Study of the Earth's short-scale gravity field using the ERTM2160 gravity model. Computer & Geosciences, 73, 71–80.

Huang D., Gubbins D., Clark R.A., Whaler K.A., 1995. Combined study of Euler's homogeneity equation for gravity and magnetic field. 57th EAGE Conference and Exhibition.

Huang L., Zhang H., Sekelani S., Wu Z., 2019. An improved tilt-Euler deconvolution and its application on a Fe-polymetallic deposit. Ore Geology Reviews, 114(103114), 1–9.

Jiang W., Zhang J., Tian T., Wang X., 2012. Crustal structure of Chuan-Dian region derived from gravity data and its tectonic implications. Physics of the Earth and Planetary Interiors, 212–213, 76–87.

Kamto P.G., Oksum E., Yap L., Kande L.H., Kamguia J., 2023. High precision structural mapping using advanced gravity processing methods: a case study from the North region of Cameroon. Acta Geophysica, 1–18.

Khakim M.Y.N., Supardi S., Tsuji T., 2023. Earthquake affects subsidence in Jakarta using Sentinel1A time series images and 2D-MSBAS method. Vietnam J. Earth Sci., 45(1), 111–130.

Konopka G., Szamałek K., Zglinicki K., 2022. Ni-Co bearing laterites from Halmahera Island (Indonesia). Applied Sciences, 12(15), 1–30.

Li Z., Liu F., Peng X., Hu B., Song X., 2022. Synergetic use of DEM derivatives, Sentinel-1 and Sentinel-2 data for mapping soil properties of a sloped cropland based on Bayesian spatial approach. Science of the Total Environment, 866, 161421.

Marson I., Klingele E.E., 1993. Advantages of using the vertical gradient of gravity for 3D interpretation. Geophysics, 58(11), 1588–1595.

Mccaffrey R., Silver E.A., Rait R.W., 1980. Crustal structure of the Molucca Sea collision zone, Indonesia. In: the tectonic and geologic evolution of Southeast Asian Seas and Islands. AGU, Washington D.C., 23, 161–177.

Menichetti M., Roccheggiani M., De Guidi G., Carnemolla F., Brighenti F., Barreca G., Monaco C., 2023. Sentinel-1 Interferometry and UAV aerial survey for mapping coseismic ruptures: Mts. Sibillini vs. Mt. Etna Volcano. Remote Sensing, 15(10), 1–29.

Milsom J., 2001. Subduction in eastern Indonesia: how many slabs?. Tectonophysics, 338(2), 167–178.

Mohcine C., Abderrazak E.H., Rachid L., Jaouad E.H., Amine J., Zakaria A., 2022. Assessment of radarsat-1, ALOS PALSAR and sentinel-1 SAR satellite images for geological lineament mapping. Geocarto International, 37(27), 15530–15547.

National Disaster Management Authority (BNPB) of Republic Indonesia., 2022. Earthquake 5.2 magnitude in North Halmahera Regency, North Maluku Province (Update: Tuesday, April 19). retrieved from https://pusdalops.bnpb.go.id/2022/04/19/gempa-bumi-5-2-sr-di-kab-halmahera-utara-prov-maluku-utara-update-selasa-19-april/

Nigussie W., Alemu A., Mickus K., Muluneh A.A., 2022. Structure of the upper crust at the axis segmentation stage of rift evolution as revealed by gravity data: Case study of the Gedemsa magmatic segment, Main Ethiopian Rift. Journal of African Earth Sciences, 190(104523), 1–11.

Nzeuga A.R., Ghomsi F.E., Pham L.T., Eldosouky A.M., Aretouyap Z., Kana J.D., Yasmine Z. T., Fokem A.B.K., Nouayou R., Abdelrahman K., Fnais M.S., Andrá P., 2022. Contribution of advanced edge-detection methods of potential field data in the tectono-structural study of the southwestern part of Cameroon. Frontiers in Earth Science, 10, 1–15.

Oksum E., Le D.V., Vu M.D., Nguyen T.H.T., Pham L.T., 2021. A novel approach based on the fast sigmoid function for interpretation of potential field

data. Bollettino di Geofisica Teorica ed Applicata, 62, 543−556.

Patria A., Tsutsumi H., Natawidjaja D.H., 2021. Active fault mapping in the onshore northern Banda Arc, Indonesia: Implications for active tectonics and seismic potential. Journal of Asian Earth Sciences, 218, 104881.

Pham L.T., 2021. A high resolution edge detector for interpreting potential field data: A case study from the Witwatersrand Basin, South Africa. Journal of African Earth Sciences, 178(104190), 1−8.

Pham L.T., Eldosouky A.M., Oksum E., Saada S.A., 2022. A new high resolution filter for source edge detection of potential field data. Geocarto International, 37(11), 3051-3068.

Pham L.T., Ghomsi F.E.K., Vu T.V, Oksum E., Steffen R., Tenzer R., 2023. Mapping the structural configuration of the western Gulf of Guinea using advanced gravity interpretation methods. Physics and Chemistry of the Earth, 129(103341), 1−12.

Prasad K.N.D., Pham L.T., Singh A.P., Eldosouky A.M., Abdelrahman K., Fnais M.S., Gómez-Ortiz D., 2022. A Novel Enhanced Total Gradient (ETG) for Interpretation of Magnetic Data. Minerals, 12, 1468.

Puspito T., Hirahara K., 1993. Three-dimensional P-wave velocity structure beneath the Indonesian region. Tectonophysics, 220(1−4), 175−92.

Rachman G., Santosa B.J., Nugraha A.D., Rohadi S., Rosalia S., Zulfakriza Z., Sungkono S., Sahara D.P., Muttaqy F., Supendi P., Ramdhan M., Ardianto A., Afif H., 2022. Seismic Structure Beneath the Molucca Sea Collision Zone from Travel Time Tomography Based on Local and Regional BMKG Networks. Applied Sciences, 12(10520), 1−21.

Rangin C., Le Pichon X., Mazzotti S., Pubellier M., Chamot-Rooke N., Aurelio M., Walpersdorf A., Quebral R., 1999. Plate convergence measured by GPS across the Sundaland/Philippine Sea Plate deformed boundary: The Philippines and eastern Indonesia. Geophysical Journal International, 139(2), 296−316.

Reid A.B., Allsop J.M., Granser H., Millettg A.J., Somerton I.W., 1990. Magnetic interpretation in three dimensions using Euler deconvolution. Geophysics, 55(1), 80−91.

Reid A.B., Thurston J.B., 2014. The structural index in gravity and magnetic interpretation: errors, uses, and abuses. Geophysics, 79(4), J61−J66.

Silver E.A., Moore J.C., 1978. The Molucca Sea collision zone, Indonesia. Journal of Geophysical Research Solid Earth, 83(8), 1681−1691.

Spector A., Grant F.S., 1970. Statistical models for interpreting aeromagnetic data. Geophysics, 35, 293−302.

Stavrev P., Reid A., 2007. Degrees of homogeneity of potential fields and structural indices of Euler deconvolution. Geophysics, 72(1), 1−12.

Sukamto, Samodra H., 1995. Geological Map of Indonesia, Morotai Sheet. Geological Research and Development Centre, Bandung.

Thompson D.T., 1982. EULDPH: A new technique for making depth estimates from magnetic data. Geophysics, 47(1), 31−37.

Thurston J.B., Smith R.S., 1997. Automatic conversion of magnetic data to depth, dip, and susceptibility contrast using the SPI (TM) method. Geophysics, 62(3), 807−813.

Vajedian S., Aflaki M., Mousavi Z., Ghods A., Walker R., Maurer J., 2023. Seismotectonic modeling of the 2017 Hojedk (Kerman) earthquake sequence from joint inversion of InSAR and offset tracking techniques. Remote Sensing of Environment, 288(113461), 1−18.

van Bemmelen R.W., 1949. General Geology of Infonesia and Adjacent Archipelagoes. Government printing office.

van Gorsel J.T., 2018. Bibliography of the geology of Indonesia and surrounding areas, edition 7.0, VI. North Moluccas, 1261p.

Waltham D., Hall R., Smyth H.R., Ebinger C.J., 2008. Basin formation by volcanic arc loading. Special Paper of the Geological Society of America, 436, 11−26.

Yamaguchi Y., 1985. Image-Scale and Look-Direction Effects on the Detectability of Lineaments in Radar Images. 127, 117−127.

Zenonos A., Siena L.D., Widiyantoro S., Rawlinson N., 2019. P and S wave travel time tomography of the SE Asia-Australia collision zone. Physics of the Earth and Planetary Interiors, 293(106267), 1−14.

Zhang Q., Guo F., Zhao L., Wu Y., 2017. Geodynamics of divergent double subduction: 3-D numerical modeling of a cenozoic example in the Molucca Sea region, Indonesia. Journal of Geophysical Research: Solid Earth, 122(5), 3977−3998.

Zhao F., Gong W., Tang H., Pudasaini S.P., Ren T., Cheng Z., 2023. An integrated approach for risk assessment of land subsidence in Xi'an, China using optical and radar satellite images. Engineering Geology, 314(106983), 1−14.